Poly(vinyl pyrrolidone): A Dual Functional Reductant and Stabilizer for the Facile Synthesis of Noble Metal Nanoplates in Aqueous Solutions

Yujie Xiong,† Isao Washio,† Jingyi Chen,† Honggang Cai,† Zhi-Yuan Li,‡ and Younan Xia*,†

Department of Chemistry, University of Washington, Seattle, Washington 98195-1700, and Institute of Physics, Chinese Academy of Sciences, Beijing 100080, People's Republic of China

Received May 10, 2006. In Final Form: July 10, 2006

Poly(vinyl pyrrolidone) (PVP) has been extensively used in the solution-phase synthesis of many types of colloidal particles, where it is mainly considered as a steric stabilizer or capping agent with a major role to protect the product from agglomeration. In a recent study, we discovered that the hydroxyl end groups of PVP could also serve as a very mild reductant for kinetically controlled synthesis of Ag nanoplates with yields as high as 75%. Here we further demonstrate that hydroxyl-terminated PVP is also a well-suited reductant for the aqueous synthesis of circular, triangular, and hexagonal nanoplates made of other noble metals including Pd, Au, and Pt. The reduction kinetics of a metal salt by the hydroxyl end groups of PVP can be maneuvered in at least two different ways to facilitate the evolution of plate morphology: (i) by adjusting the molar ratio of PVP to the salt precursor and (ii) by altering the molecular weight of PVP. Unlike previously reported studies of Ag and Au thin plates, light was found to have a negligible role in the present synthesis.

1. Introduction

Metal nanostructures have been of great interest for decades because of their use in catalysis, photography, photonics, electronics, plasmonics, information storage, labeling, imaging, sensing, and surface-enhanced Raman scattering (SERS).[1−6] Most of these applications are derived from the conduction electrons intrinsic to metal nanostructures. For example, the collective oscillation of conduction electrons in Au and Ag nanostructures results in surface plasmon resonance (SPR), enabling their extensive use in plasmonics, optical sensing, and SERS. As confirmed by various studies, the SPR properties of a metal nanostructure are strongly dependent on parameters such as the size, shape, composition, crystallinity, and structure (e.g., solid vs hollow).[7] In many cases, it is necessary to control these parameters in order to tailor the SPR features and thus optimize a specific application.

Shape control has recently received considerable attention because it allows one to tune the surface plasmonic bands with greater versatility than can be achieved otherwise.[8] For instance, the SPR properties of Pd nanoparticles have been largely unexplored up till a few years ago, mainly because the SPR peaks of Pd nanoparticles (cubooctahedral or twinned, typically <10 nm in size) are located in the UV region and it is very difficult to probe them as a result of the strong absorption of light by glass and most solvents.[9] By making this material into triangular and hexagonal nanoplates, we recently demonstrated that the SPR peaks could be shifted from 225 to 530 nm.[10a] As a result, now it becomes possible to explore the use of Pd nanostructures in applications such as sensing and SERS.[10] Thanks to the efforts from many research groups, shape-controlled synthesis has been achieved for a number of metals and alloys, including Co, Ag, Au, Pt, Pd, Rh, and FePt.[8,9,10a,11] Among various shapes, nanoplates[12] have drawn particular attention, as they have sharp corners and edges that are supposed to be most active

* Corresponding author. e-mail xia@chem.washington.edu.
† University of Washington.
‡ Chinese Academy of Sciences.

(1) General: (a) Halperin, W. P. *Rev. Mod. Phys.* **1986**, *58*, 533. (b) Henglein, A. *Chem. Rev.* **1989**, *89*, 1861. (c) Kreibig, U.; Vollmer, M. *Optical Properties of Metal Clusters*; Springer: New York, 1995. (d) Templeton, A. C.; Wuelfing, W. P.; Murray, R. W. *Acc. Chem. Res.* **2000**, *33*, 27.

(2) Catalysis: Lewis, L. N. *Chem. Rev.* **1993**, *93*, 2693.

(3) Photography and photonics: (a) Lam, D. M.-K.; Rossiter, B. W. *Sci. Am.* **1991**, *265*, 80. (b) El-Sayed, M. A. *Acc. Chem. Res.* **2001**, *34*, 257. (c) Maier, S. A.; Brongersma, M. L.; Kik, P. G.; Meltzer, S.; Requicha, A. A. G.; Atwater, H. A. *Adv. Mater.* **2001**, *13*, 1501. (d) Murphy, C. J.; Jana, N. R. *Adv. Mater.* **2002**, *14*, 80. (e) Chen, S.; Yang, Y. *J. Am. Chem. Soc.* **2002**, *124*, 5280. (f) Teng, X.; Black, D.; Watkins, N. J.; Gao, Y.; Yang, H. *Nano Lett.* **2003**, *3*, 261.

(4) Information storage: Peyser, L. A.; Vinson, A. E.; Bartko, A. P.; Dickson, R. M. *Science* **2001**, *291*, 103.

(5) Labeling, imaging, and sensing: (a) Taton, T. A.; Mirkin, C. A.; Letsinger, R. L. *Science* **2000**, *289*, 1757. (b) Nicewarner-Peña, S. R.; Freeman, R. G.; Reiss, B. D.; He, L.; Peña, D. J.; Walton, I. D.; Cromer, R.; Keating, C. D.; Natan, M. J. *Science* **2001**, *294*, 137. (c) Tkachenko, A. G.; Xie, H.; Coleman, D.; Glomm, W.; Ryan, J.; Anderson, M. F.; Franzen, S.; Feldheim, D. L. *J. Am. Chem. Soc.* **2003**, *125*, 4700. (d) Zhang, X.; Young, M. A.; Lyandres, O.; Van Duyne, R. P. *J. Am. Chem. Soc.* **2005**, *127*, 4484. (e) Chen, J.; Saeki, F.; Wiley, B. J.; Cang, H.; Cobb, M. J.; Li, Z.-Y.; Au, L.; Zhang, H.; Kimmey, M. B.; Li, X.; Xia, Y. *Nano Lett.* **2005**, *5*, 473.

(6) SERS: (a) Jeanmaire, D. L.; Van Duyne, R. P. *J. Electroanal. Chem.* **1977**, *84*, 1. (b) Nie, S.; Emory, S. R. *Science* **1997**, *275*, 1102. (c) Tessier, P. M.; Velev, O. D.; Kalambur, A. T.; Rabolt, J. F.; Lenhoff, A. M.; Kaler, E. W. *J. Am. Chem. Soc.* **2000**, *122*, 9554. (d) Cao, Y. C.; Jin, R.; Mirkin, C. A. *Science* **2002**, *297*, 1536. (e) Haes, A. J.; Haynes, C. L.; McFarland, A. D.; Schatz, G. C.; Van Duyne, R. P.; Zhou, S. *MRS Bull.* **2005**, *30*, 368.

(7) (a) Jackson, J. B.; Halas, N. J. *J. Phys. Chem. B* **2001**, *105*, 2473. (b) Sun, Y.; Xia, Y. *J. Am. Chem. Soc.* **2004**, *126*, 3892. (c) Xiong, Y.; Wiley, B.; Chen, J.; Li, Z.-Y.; Yin, Y.; Xia, Y. *Angew. Chem., Int. Ed.* **2005**, *44*, 7913.

(8) (a) Chen, S.; Wang, Z. L.; Ballato, J.; Foulger, S. H.; Carroll, D. L. *J. Am. Chem. Soc.* **2003**, *125*, 16186. (b) Caswell, K. K.; Wilson, J. N.; Bunz, U. H. F.; Murphy, C. J. *J. Am. Chem. Soc.* **2003**, *125*, 13914. (c) Kim, F.; Connor, S.; Song, H.; Kuykendall, T.; Yang, P. *Angew. Chem., Int. Ed.* **2004**, *43*, 3673. (d) Narayanan, R.; El-Sayed, M. A. *J. Phys. Chem. B* **2004**, *108*, 5726. (e) Hao, E.; Bailey, R. C.; Schatz, G. C.; Hupp, J. T.; Li, S. *Nano Lett.* **2004**, *4*, 327.

(9) (a) Creighton, J. A.; Eadon, D. G. *J. Chem. Soc., Faraday Trans.* **1991**, *87*, 3881. (b) Xiong, Y.; Chen, J.; Wiley, B.; Xia, Y.; Aloni, S.; Yin, Y. *J. Am. Chem. Soc.* **2005**, *127*, 7332. (c) Xiong, Y.; Chen, J.; Wiley, B.; Xia, Y.; Yin, Y.; Li, Z.-Y. *Nano Lett.* **2005**, *5*, 1237.

(10) (a) Xiong, Y.; McLellan, J. M.; Chen, J.; Yin, Y.; Li, Z.-Y.; Xia, Y. *J. Am. Chem. Soc.* **2005**, *127*, 17118. (b) McLellan, J.; Xiong, Y.; Hu, M.; Xia, Y. *Chem. Phys. Lett.* **2006**, *417*, 230.

(11) (a) Sun, S.; Murray, C. B.; Weller, D.; Folks, L.; Moser, A. *Science* **2000**, *287*, 1989. (b) Chen, J.; Herricks, T.; Xia, Y. *Angew. Chem., Int. Ed.* **2004**, *44*, 2. (c) Gugliotti, L. A.; Feldheim, D. L.; Eaton, B. E. *Science* **2004**, *304*, 850. (d) Yin, Y.; Alivisatos, A. P. *Nature* **2005**, *437*, 664.

10.1021/la061323x CCC: $33.50
Published on Web 08/31/2006

Scheme 1. Formulas of OH-Terminated Poly(vinyl pyrrolidone) (PVP) and Its Structural Changes Involved in the Oxidation by Various Noble Metal Ions.

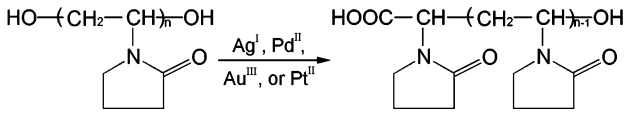

for SERS (where the local electromagnetic field could be enhanced more than 500 times[13]).

Most of the shape-controlled syntheses involve the reduction of salt precursors or thermal decomposition of organometallic compounds in the presence of organic surfactants, polymers, biomacromolecules, and coordinating ligands, and sometimes with the mediation of ionic species. Another simple and versatile route toward shape-controlled synthesis of metal nanocrystals is based on kinetic control.[10a,11b] For a face-centered cubic (fcc) noble metal, truncated nanocubes (or cubooctahedra) and multiple twinned particles (MTPs) have the lowest free energy and are therefore favored by thermodynamics.[9b,14] To obtain a shape other than the thermodynamic ones, the kinetics of nucleation must be carefully controlled. Specifically, when the reduction of metal species and the generation of metal atoms become substantially slow, the nucleation and growth can be turned into kinetic control. Previously we have employed such kinetic control to obtain a variety of Pd and Pt nanostructures by coupling polyol reduction with oxidative etching, in which the reduction was retarded for various periods of time.[10a,11b] In this paper, we demonstrate that the reduction kinetics can be controlled not only through the introduction of an oxidative etchant to compete with the reduction but also through modification to the reductant.

Alcohol reduction has been known for decades as a generic route to the synthesis of metal colloids.[9−11,14,15] It is also known that the reducing power of an alcohol decreases as its alkyl chain becomes longer. As a result, polymers with hydroxyl (-OH) end groups would be ideal reductants for kinetically controlled synthesis of metal nanostructures. Poly(vinyl pyrrolidone) (PVP, see Scheme 1) has been widely used in the chemical synthesis of many types of colloidal nanocrystals. The major role of PVP has been assigned as a steric stabilizer or capping agent to protect the product from agglomeration.[9−11,14,16] It has been somehow ignored by the colloidal community that the ends of commercially available PVP are terminated in the hydroxyl group due to the involvement of water and hydrogen peroxide in polymerization.[17] Although Kan et al.[16g] mentioned the reduction power of PVP, they did not identify the role of its end groups. Most recently we discovered that such a polymer could act like a long-chain alcohol and serve as a new class of reductant whose mild reducing power is instrumental in the kinetically controlled synthesis of Ag nanoplates.[18] Here we demonstrate that reduction of metal salts by the hydroxyl end groups of PVP can be applied as a general strategy for the kinetically controlled synthesis of nanoplates made of other noble metals such as Pd, Au, and Pt. As a major advantage over alcohols with short alkyl chains commonly used in the conventional synthesis, the PVP can work as both reductant and stabilizer.

2. Experimental Section

Chemicals and Materials. Silver nitrate ($AgNO_3$, 209139, 100 g), sodium palladium(II) tetrachloride (Na_2PdCl_4, 379808, 1 g), hydrogen tetrachloroaurate(III) ($HAuCl_4$, 484385, 1 g), and PVP (MW = 10 000, 29 000, and 55 000) were all received from Aldrich and used without further purification. The water used in all reactions was obtained by filtering through a set of Millipore cartridges (E-pure, Dubuque, IA).

Synthesis of Silver Nanoplates. In each synthesis, a specific amount of PVP was dissolved in 8.0 mL of water hosted in a 20-mL vial (liquid scintillation vial with polyethylene liner and a white cap, Research Products International Corp.), and heated to 60 °C in air under magnetic stirring. Meanwhile, 3.0 mL of an aqueous $AgNO_3$ solution (188 mM) was rapidly added into the vial. For PVP of each molecular weight, the molar ratio between the repeating unit of PVP and $AgNO_3$ was varied from 30 to 15 and 5. After the vial had been capped, the reaction mixture was continued with heating at 60 °C in air for 21 h. At different stages of the reaction, samples were taken from the solution with a glass pipet, centrifuged, and then washed with water three times to remove excess PVP.

Synthesis of Palladium Nanoplates. In each synthesis, PVP was dissolved in 8.0 mL of water hosted in a 25-mL, three-neck flask (equipped with a reflux condenser and a Teflon-coated magnetic stirring bar), and heated to 80 °C in air under magnetic stirring. Meanwhile, 3.0 mL of an aqueous solution of Na_2PdCl_4 (21.4 mM) was rapidly added to the flask. For PVP of each molecular weight, the molar ratio between the repeating unit of PVP and $AgNO_3$ was varied from 15 to 5 and 1.5. The reaction mixture was heated at 80 °C in air for 5 h before the product was collected by centrifugation and washed (one time) with acetone and finally with ethanol three times to remove excess PVP.

Synthesis of Gold Microplates. In each synthesis, 0.1000 g of PVP (MW = 29 000) was dissolved in 8.0 mL of water hosted in a 25-mL, three-neck flask (equipped with a reflux condenser and a Teflon-coated magnetic stirring bar) and heated to 65 °C in air under magnetic stirring. Meanwhile, 3.0 mL of an aqueous $HAuCl_4$ solution (20.0 mM) was rapidly added into the flask. The reaction mixture was heated to 65 °C in air for 15 min before the product was centrifuged and washed with acetone and then with ethanol three times to remove excess PVP.

Instrumentation. Transmission electron microscopy (TEM) images and electron diffraction (ED) patterns were captured on a Philips 420 microscope operated at 120 kV. Scanned electron microscopy (SEM) images were taken on a FEI field-emission microscope (Sirion XL) operated at an accelerating voltage of 20 kV. Samples for TEM and SEM studies were prepared by drying a drop of the aqueous suspension of particles on a piece of carbon-coated copper grid (Ted Pella, Redding, CA) or silicon wafer under ambient conditions. The TEM grid or silicon wafer was then transferred to a gravity-fed flow cell and washed for 1 h with deionized water to remove excess PVP. Finally, the sample was dried and

(12) (a) Jin, R.; Cao, Y.; Mirkin, C. A.; Kelly, K. L.; Schatz, G. C.; Zheng, J. G. *Science* **2001**, *294*, 1901. (b) Chen, S.; Carroll, D. L. *Nano Lett.* **2002**, *2*, 1003. (c) Pastoriza-Santos, I.; Liz-Marzán, L. M. *Nano Lett.* **2002**, *2*, 903. (d) Maillard, M.; Giorgio, S.; Pileni, M.-P. *Adv. Mater.* **2002**, *14*, 1084. (e) Jin, R.; Cao, Y. C.; Hao, E.; Metraux, G. S.; Schatz, G. C.; Mirkin, C. A. *Nature (London)* **2003**, *425*, 487. (f) Sun, Y.; Xia, Y. *Adv. Mater.* **2003**, *15*, 695. (g) Sun, X.; Dong, S.; Wang, E. *Angew. Chem., Int. Ed.* **2004**, *43*, 6360. (h) Ah, C. S.; Yun, Y. J.; Park, H. J.; Kim, W.-J.; Ha, D. H.; Yun, W. S. *Chem. Mater.* **2005**, *17*, 5558.

(13) Kelly, K. L.; Coronado, E.; Zhao, L. L.; Schatz, G. C. *J. Phys. Chem. B* **2003**, *107*, 668.

(14) (a) Wiley, B.; Herricks, T.; Sun, Y.; Xia, Y. *Nano Lett.* **2004**, *4*, 1733. (b) Wiley, B.; Sun, Y.; Mayers, B.; Xia, Y. *Chem.—Eur. J.* **2005**, *11*, 455.

(15) (a) Rampino, L. D.; Nord, F. F. *J. Am. Chem. Soc.* **1942**, *63*, 2745. (b) Fievet, F.; Lagier, J. P.; Figlarz, M. *MRS Bull.* **1989**, 29. (c) Ayyappan, S.; Gopalan, R. S.; Subbanna, G. N.; Rao, C. N. R. *J. Mater. Res.* **1997**, *12*, 398. (d) Teranishi, T.; Hosoe, M.; Tanaka, T.; Miyake, M. *J. Phys. Chem. B* **1999**, *103*, 3818. (e) Wang, Y.; Ren, J.; Deng, K.; Gui, L.; Tang, Y. *Chem. Mater.* **2000**, *12*, 1622. (f) Narayanan, R.; El-Sayed, M. A. *J. Phys. Chem. B* **2003**, *107*, 12416. (g) Yamamoto, T.; Wada, Y.; Sakata, T.; Mori, H.; Goto, M.; Hibino, S.; Yanagida, S. *Chem. Lett.* **2004**, *33*, 158. (h) Kim, K.-S.; Choi, S.; Cha, J.-H.; Yeon, S.-H.; Lee, H. *J. Mater. Chem.* **2006**, *16*, 1315.

(16) (a) Duff, D. G.; Baiker, A.; Edwards, P. *Langmuir* **1993**, *9*, 2301. (b) Zhang, Z.; Zhao, B.; Hu, L. *J. Solid State Chem.* **1996**, *121*, 105. (c) Huang, H. H.; Ni, X. P.; Loy, G. L.; Chew, C. H.; Tan, K. L.; Loh, F. C.; Deng, J. F.; Xu, G. Q. *Langmuir* **1996**, *12*, 909. (d) Agt, P. Y.; Urbina, R. H.; Elhsissen, K. T. *J. Mater. Chem.* **1997**, *7*, 293. (e) Bonet, F.; Tekaia-Elhsissen, K.; Sarathy, K. V. *Bull. Mater. Sci.* **2000**, *23*, 165. (f) Pastoriza-Santos, I.; Liz-Marzán, L. M. *Nano Lett.* **2002**, *2*, 903. (g) Kan, C.; Cai, W.; Li, C.; Zhang, L. *J. Mater. Res.* **2005**, *20*, 320.

(17) (a) Reppe, W. *Polyvinylpyrrolidone*; Verlag: Weinheim, Germany, 1954. (b) Raith, K.; Kühn, A. V.; Rosche, F.; Wolf, R.; Neubert, R. H. H. *Pharm. Res.* **2002**, *19*, 556.

(18) Washio, I.; Xiong, Y.; Yin, Y.; Xia, Y. *Adv. Mater.* **2006** (in press).

stored in a vacuum for TEM and SEM characterization. Ultraviolet−visible−near-infrared (UV−vis−NIR) extinction spectra were taken at room temperature on a Cary 5E (Varian) spectrophotometer by use of methacrylate cuvettes (Fisher Scientific) with an optical path length of 1 cm. Powder X-ray diffraction (PXRD) patterns were recorded on a Philips 1820 diffractometer with a Cu Kα radiation source (λ = 1.541 80 Å).

The conversion percentage of salt precursor to metal in a synthesis was determined by atomic emission spectroscopy (AES). The AES measurements were performed on a Jarrell-Ash 955 Plasma AtomComp atomic emission spectrometer. In a typical procedure, the solid product from a synthesis was collected by centrifugation and then dissolved in an aqueous HNO_3 solution (with a concentration of 63%). The solution was diluted to the level of 1−10 ppm and then subjected to AES measurements. The emission lines at 328.0 and 340.5 nm were used to determine the concentrations of Ag and Pd atoms, respectively. The conversion percentage was calculated on the basis of the amount of metal atoms contained in the HNO_3 solution and the amount of metal salt initially added to the synthetic solution.

3. Results and Discussion

Stacking faults are involved in (and probably responsible for) the growth of both Au and Ag nanoplates.[12,19,20] Because of such defects, nanoplates are intrinsically higher in energy than the thermodynamically favored shapes (e.g., truncated cubes and multiple twinned particles), and their formation becomes favorable only in a slow reduction process. As a result, one must have good control over the reduction kinetics, particularly in the nucleation stage, to generate such highly anisotropic nanostructures.[21] When the reduction becomes slow enough, kinetic control will take over in both nucleation and growth: seeds with stacking faults can nucleate and then grow into nanoplates. In contrast, when the reduction is fast, the seeds will evolve into other structures instead of nanoplates, regardless of the stacking faults. In the last several years, kinetic control has been demonstrated as a simple and versatile approach to the shape-controlled synthesis of metal nanostructures. In the synthesis of Ag nanoplates, for example, Ostwald ripening involved in photoinduced or thermally induced transformation was found to be sufficiently slow to ensure kinetic control.[12a−e] Most recently, we have also employed such kinetic control to accomplish synthesis of Pd triangular and hexagonal nanoplates by coupling oxidative etching with polyol reduction.[10a] In the present work, the mild reducing power of PVP seems to be the most important factor in kinetically controlling the nucleation and growth of metal nanoplates. The reduction kinetics can be further maneuvered by controlling the molar ratio of PVP to metal salts and the molecular weight of PVP. On the other hand, both oxygen and nitrogen atoms of the pyrrolidone unit can facilitate the adsorption of PVP onto the surface of metal nanostructures, making PVP a good stabilizer to protect the product from agglomeration.[16]

Table 1 summarizes the products obtained under different experimental conditions, including the molecular weight of PVP, the molar ratio of PVP to the metal precursor, reaction temperature, and time. Detailed descriptions are provided below.

Formation of Silver Nanoplates. As briefly discussed in a recent communication from our group, the slow reduction of $AgNO_3$ by the hydroxyl end groups of PVP is instrumental in the formation of Ag nanoplates.[18] Figure 1A−D shows SEM images of four typical samples that were taken at different stages of a synthesis, in which the PVP had an average molecular weight of 29 000 and its molar ratio (calculated in terms of the repeating unit) to $AgNO_3$ was kept at 30. The nanoplates had a circular cross-section in the early stage of the reaction; they evolved into hexagons and then triangles as their lateral dimensions were increased from 50 to 350 nm. It is worth pointing out that the size uniformity of nanoplates was gradually improved with reaction time, and this observation can probably be attributed to the involvement of Ostwald ripening in the growth process. Extinction spectra taken from these solutions show that the position of the in-plane SPR peak gradually red-shifted to the

Table 1. Summary of Products Obtained under Different Experimental Conditions

metal precursor	MW of PVP	molar ratio, PVP:metal precursor	temp, °C	time	shape, average size, and yield of plates[a]
$AgNO_3$	55 000	5	60	21 h	triangular, 180 nm, 15%
$AgNO_3$	55 000	15	60	21 h	triangular, 180 nm, 20%
$AgNO_3$	55 000	30	60	21 h	triangular, 180 nm, 28%
$AgNO_3$	29 000	30	60	21 h	triangular, 350 nm, 75%
$AgNO_3$	10 000	30	60	21 h	triangular, 400 nm, 15%
Na_2PdCl_4	55 000	1.5	80	5 h	hexagonal, 40 nm, 10%
Na_2PdCl_4	55 000	5	80	5 h	hexagonal, 45 nm, 70%; triangular, 40 nm, 20%
Na_2PdCl_4	55 000	15	80	5 h	hexagonal, 45 nm, 60%; triangular, 25 nm, 30%
Na_2PdCl_4	29 000	15	80	5 h	triangular, 10 nm, 40%; hexagonal, 40 nm, 20%
Na_2PdCl_4	10 000	15	80	5 h	triangular, 50 nm, 70%
Na_2PdCl_4	55 000	5	95	5 h	hexagonal, 30 nm, 30%; triangular, 30 nm, 20%
$HAuCl_4$	29 000	15	65	15 min	hexagonal, 800 nm, 30%; triangular, 800 nm, 20%
Na_2PtCl_4	55 000	5	80	5 h	triangular, 15 nm, 20%

[a] Yield = the percentage of plates in the products.

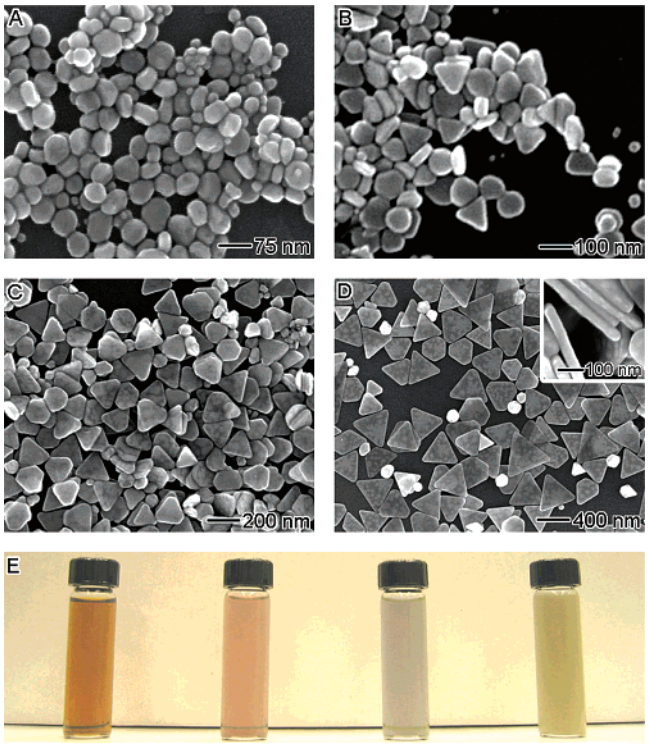

Figure 1. SEM images of Ag nanoplates sampled at different stages of a synthesis: (A) t = 20 min, (B) t = 1 h, (C) t = 3 h, and (D) t = 21 h. (D, inset) SEM image taken from a tilted sample. (E) Photograph of the reaction solution at stages corresponding to the images shown in panels A−D. The synthesis was conducted at 60 °C. The PVP had an average molecular weight of 29 000, and its molar ratio (in terms of repeating unit) to $AgNO_3$ was 30.

(19) (a) Kirkland, A. I.; Jefferson, D. A.; Duff, D. G.; Edwards, P. P.; Gameson, I.; Johnson, B. F. G.; Smith, D. J. *Proc. R. Soc. London, A* **1993**, *440*, 589. (b) Germain, V.; Li, J.; Ingert, D.; Wang, Z. L.; Pileni, M. P. *J. Phys. Chem. B* **2003**, *107*, 8717.
(20) Lofton, C.; Sigmund, W. *Adv. Funct. Mater.* **2005**, *15*, 1197.
(21) Mullin, J. W. *Crystallization*; Butterworth: London, 1961.

near-IR region as the reaction time was prolonged, implying a strong size dependence for the in-plane SPR band. Figure 1E shows photographs of the solution taken at four different stages corresponding to panels A−D. It is clear that the color of the Ag nanoplates could be tuned from orange to blue and gray by simply controlling the reaction time. As a result, one can use this synthetic protocol to prepare Ag nanoplates with well-controlled SPR features tunable in the visible and near-IR regions.

In the synthesis, the $AgNO_3$ was reduced by the end groups of PVP. As reported in the literature, the ends of commercial PVP are usually terminated in the hydroxyl group (-OH) when water is used as the solvent for polymerization and hydrogen peroxide is involved.[17] The hydroxyl end groups have been clearly identified from the ^{13}C NMR spectrum of PVP with a relatively low molecular weight (∼10 000).[18] The conversion percentage from $AgNO_3$ to Ag was also found to be directly proportional to the concentration of hydroxyl end groups of PVP, a parameter that can be conveniently adjusted by varying the molar ratio of PVP to $AgNO_3$ and/or the molecular weight of PVP.[18] These experimental results clearly demonstrated that the hydroxyl end groups of PVP serve as the reductant in the synthesis of Ag nanoplates.

The reduction rate, and thus the morphology of final product, can be controlled by adjusting a number of parameters. In general, the reduction became faster as the concentration of hydroxyl end groups was increased. Table 1 summarizes all the morphologies that have been observed under different experimental conditions. The product morphology also depended on temperature in two different ways. First, as described above, slower reduction at lower temperatures was beneficial to the kinetic control and thus formation of nanoplates at higher yields. Second, an extremely slow reaction would continuously generate Ag atoms over a long period of time and suppress Ostwald ripening, resulting in size polydispersity. When these factors are taken together, the reduction rate should be kept at a moderate level by adjusting temperature in order to achieve size uniformity.

Formation of Palladium Nanoplates. Although the reduction of Na_2PdCl_4 by the hydroxyl end groups of PVP proceeds in a way similar to the silver system, Pd hexagonal and triangular nanoplates could be selectively formed. In this case, the reduction kinetics could also be easily manipulated by varying the molar ratio of PVP to Na_2PdCl_4 and the molecular weight of PVP. Palladium hexagonal nanoplates were obtained when the molar ratio of PVP (MW = 55 000) to Pd precursor was adjusted to 5. Figure 2 shows SEM and TEM images of the as-prepared hexagonal nanoplates. Their average edge length was 45 nm, and their thickness was estimated to be ∼8 nm from the SEM image of tilted nanoplates (see the inset of Figure 2A). The inset of Figure 2C shows a typical electron diffraction (ED) pattern recorded by directing the electron beam perpendicular to the hexagonal flat faces of an individual nanoplate. The 6-fold rotational symmetry of the diffraction spots implies that the hexagonal faces are presented by the {111} planes. Three sets of spots can be identified on the basis of their *d* spacings: the outer, triangled set with a lattice spacing of 0.8 Å can be indexed to the {422} Bragg reflection, the squared set with a spacing of 1.4 Å is due to the {220} reflection of face-centered cubic (fcc) Pd, and the inner set (circled) with a lattice spacing of 2.4 Å is believed to originate from the forbidden 1/3{422} reflection. The forbidden 1/3{422} reflection has also been observed for both Pd and Ag nanoplates in previous studies.[10a,12f,19] The stacking faults are responsible for the appearance of the 1/3{422} reflection.[19] The inset of Figure 2D shows a typical ED pattern from the side face recorded in the [011] orientation when the nanoplate was titled by 35°. This pattern confirms that the side faces of each nanoplate are bound by the {100} or {111} planes. These assignments are consistent with the geometrical model, in which each Pd hexagonal nanoplate is bound by two {111} planes as the top and bottom faces and a mix of {100} and {111} planes as the side faces.[10a,22]

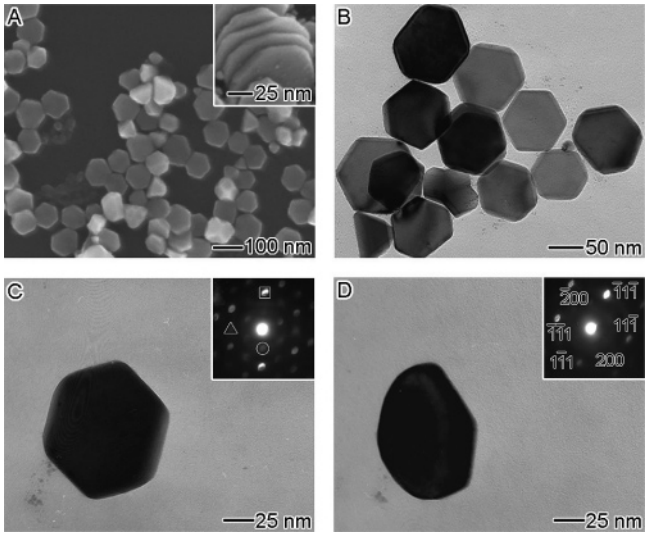

Figure 2. (A) SEM and (B) TEM images of Pd hexagonal nanoplates. The PVP had an average molecular weight of 55 000, and its molar ratio (in terms of repeating unit) to Na_2PdCl_4 was 5. The synthesis was performed at 80 °C. (A, inset) SEM image of a number of hexagonal nanoplates stacked into a column. (C) TEM image of an individual nanoplate; (inset) ED pattern recorded by directing the electron beam perpendicular to its hexagonal flat faces. (D) TEM image of the same nanoplate after it had been tilted by 35°; (inset) ED pattern taken from its edge. For the nanoplate without tilting, the strongest spots (squared) could be indexed to the allowed {220} reflection; the outer spots (triangled) with the weakest intensity could be assigned to the allowed {422} reflection; and the inner spots (circled) with a weaker intensity corresponded to the formally forbidden 1/3{422} reflection.

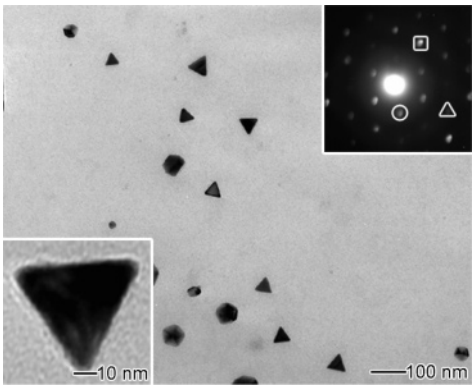

Figure 3. TEM images of Pd triangular nanoplates. The PVP had an average molecular weight of 10 000, and its molar ratio (in terms of repeating unit) to Na_2PdCl_4 was 15. The reaction was performed at 80 °C. Upper right inset) ED pattern of a triangular nanoplate recorded by directing the beam perpendicular to its triangular flat faces. The spots squared, triangled, and circled could be indexed to the {220}, {422}, and forbidden 1/3{422} reflections, respectively. (Lower left inset) TEM image at a higher magnification.

Palladium triangular nanoplates were obtained when the molar ratio of PVP (MW = 10 000) to Pd precursor was increased to 15. Figure 3 shows a TEM image of the as-synthesized triangular nanoplates with an average edge length of 50 nm. The ED pattern

(22) Wang, Z. L. *J. Phys. Chem. B* **2000**, *104*, 1153.

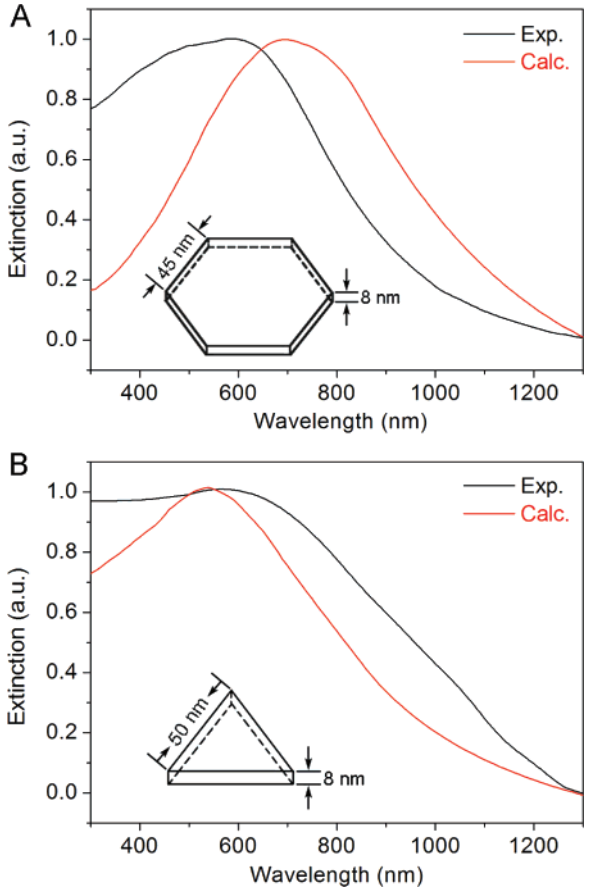

Figure 4. (A) Comparison of the UV−vis−NIR extinction spectrum of the Pd sample shown in Figure 2A with the DDA calculation performed on a Pd hexagonal nanoplate of 45 nm in edge length and 8 nm thick. (B) Comparison of the UV−vis−NIR extinction spectrum of the Pd sample shown in Figure 3 with the DDA calculation performed on a Pd triangular nanoplate 50 nm in edge length and 8 nm in thickness. The nanoplates were dispersed in water, and all random configurations of the plate with respect to the incident light were averaged. The extinction coefficients were defined as $C/\pi r_{\mathrm{eff}}^2$ (with C being the cross-sections obtained directly from DDA calculation and α_{eff} being defined through the concept of an effective volume equal to $4\pi r_{\mathrm{eff}}^3/3$ for the plate).

(upper right inset of Figure 3) is also composed of three sets of diffraction spots with 6-fold rotational symmetry, which can be indexed to be the {422}, {220}, and forbidden 1/3{422} reflections, respectively. The ED pattern suggests that each Pd triangular nanoplate is bound by two {111} planes as the top and bottom faces and three {100} planes as the side faces.

In comparison with the Pd nanoplates prepared by coupling polyol reduction with oxidative etching, the nanoplates presented here have larger sizes (45 nm for triangular nanoplates and 50 nm for hexagonal nanoplates versus 28 nm for previous work), which are supposed to exhibit more red-shifted SPR peaks. Figure 4 shows UV−vis−NIR extinction spectra recorded from aqueous suspensions of the Pd sample in Figure 2A and the sample in Figure 3 prepared by the present procedure; their SPR peaks were shifted from 520 nm (for 28-nm plates) to 610 and 600 nm, respectively. To understand these features, we calculated the spectra using the discrete dipole approximation (DDA) method. The red lines in Figure 4 show the extinction coefficients of a Pd hexagonal nanoplate 45 nm in edge length and 8 nm in thickness and a triangular nanoplate 50 nm in edge length and 8 nm in thickness, respectively.[13] Note that the broadening of these SPR peaks can be ascribed to the dielectric function of Pd, as well as the small thicknesses of the plates.[10] Compared with

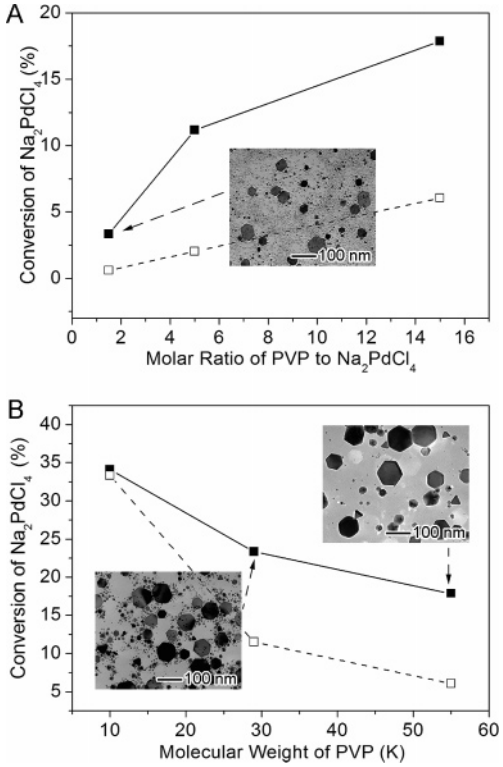

Figure 5. (A) Plot showing linear dependence of the conversion percentage of Na_2PdCl_4 to Pd on the molar ratio of poly(vinyl pyrrolidone) (PVP) (MW = 55 000) to Na_2PdCl_4. (B) Plot showing dependence of the conversion percentage of Na_2PdCl_4 to Pd on the molecular weight of PVP, with the molar ratio of PVP to Na_2PdCl_4 being kept at 15. (■) Experimental conversion percentages measured by AES; (□) stoichiometric calculations. In both cases, the molar ratio of PVP to $AgNO_3$ was calculated in terms of the repeating unit. (Insets) Typical TEM images of the samples prepared under the corresponding conditions, with all syntheses being conducted at 80 °C.

the results of DDA calculation, both samples displayed broader SPR peaks, probably due to the polydispersity of as-synthesized nanoplates. As the sample in Figure 2A also contained 20% triangular nanoplates (with SPR peaks around 500 nm) and 10% small nanoparticles (with SPR peaks in the UV region) in addition to hexagonal plates, the maximum (610 nm) of the experimentally measured peak is more blue-shifted than the position of the peak (690 nm) calculated for 45-nm hexagonal nanoplates. Similarly, the sample in Figure 3 contains 30% small nanoparticles in addition to triangular nanoplates, resulting in the shoulder at 400−600 nm. These Pd nanostructures with more red-shifted SPR bands are expected to exhibit stronger SERS activity, as their SPR maxima will interact more intensely with the laser of a commercial Raman spectroscope (785 nm).[10,23]

To elucidate the mechanism, we measured the conversion percentage of Na_2PdCl_4 to Pd by varying the molar ratio of PVP to Na_2PdCl_4, as well as the molecular weight of PVP. As shown in Figure 5A, the conversion percentage of Na_2PdCl_4 to Pd was directly proportional to the molar ratio of PVP to Na_2PdCl_4. In contrast, the conversion percentage decreased as PVPs of higher molecular weights were used (Figure 5B). These trends were similar to those observed for the Ag system.[18] However, when compared with the calculated values (as indicated by open squares in Figure 5), the experimental conversion percentages were much higher. The difference can be attributed to the autocatalytic effect,

(23) (a) Schwartzberg, A. M.; Grant, C. D.; Wolcott, A.; Talley, C. E.; Huser, T. R.; Bogomolni, R.; Zhang, J. Z. *J. Phys. Chem. B* **2004**, *108*, 19191. (b) Halas, N. *MRS Bull.* **2005**, *30*, 362.

which has been established for the nucleation and growth of noble metal clusters or nanocrystals.[24] In the present case, the precursor of Na_2PdCl_4 probably formed chainlike small clusters or complexes through the bridging of Cl^- anions,[25] which could act as nucleation sites for the autocatalytic reaction.

When the reduction kinetics was fastened by increasing the concentration of hydroxyl end groups, the Pd nanoparticles evolved from hexagonal to triangular nanoplates. This observation is consistent with the evolution of shape when the reduction rate was manipulated by coupling polyol reduction with oxidative etching.[10a] It is clear that the mild reducing power of hydroxyl end groups of PVP leads to a slow reduction rate, which is desired for kinetically controlled synthesis of Pd nanoplates. In contrast, when poly(vinyl alcohol) (PVA, MW = 88 000, where a hydroxyl group is attached to each repeating unit) was used, the product (see Figure 6A) was found to only contain 10% triangular nanoplates together with 90% truncated nanocubes and small nanoparticles. In this case, the higher concentration of hydroxyl groups resulted in a faster reduction rate and formation of thermodynamically favored shapes.

In terms of shape evolution, the nanoplates had a circular cross-section in the initial stage. As reaction time was prolonged, they evolved into hexagonal and then triangular shapes together with a large increase in their lateral dimensions. This change in cross-section was observed only in the synthesis of Ag nanoplates. For the Pd system, the reduction rate was too fast to catch the stage where only circular or hexagonal nanoplates existed. When the reduction was slowed by decreasing the PVP amount, hexagonal nanoplates were obtained. As shown in Figure 2, a small fraction of these hexagonal plates had evolved into triangular ones.

Different from the Ag system, Na_2PdCl_4 may hydrolyze while it is reduced by the hydroxyl end groups of PVP, and this side reaction may lead to the formation of palladium oxide hydrate ($PdO{\cdot}H_2O$). Figure 7A shows the PXRD pattern of the product prepared in the absence of PVP. All the peaks can be indexed to tetragonal $PdO{\cdot}H_2O$ (JCPDS card 09-0254). When the concentration of hydroxyl end groups was relatively low, the product became a mixture of Pd and $PdO{\cdot}H_2O$. Figure 7B shows the PXRD pattern of the product that was prepared with the molar ratio of PVP (MW = 55 000) to Pd precursor being reduced to 1.5. In this case, the peaks can be assigned to a mixture of Pd and $PdO{\cdot}H_2O$. As the concentration of hydroxyl end groups was increased, the product was made up purely of fcc Pd (see Figure 7C, JCPDS card 05-0681). Therefore, sufficient concentration of hydroxyl end groups is crucial to the production of pure Pd product. In the PXRD pattern for hexagonal nanoplates (Figure 7C), the ratio between the intensities of (111) and (200) peaks is higher than the index value (2.89 vs 2.38), indicating that the top and bottom faces of each nanoplate are bounded by the {111} planes. These nanoplates were more or less oriented parallel to the supporting substrate, and this texturing effect resulted in a stronger (111) diffraction peak than that of a conventional powder sample.

The selection of an appropriate temperature is also critical to the achievement of a desirable reduction rate. Similar to the Ag system, both the shape and size of the product depended on temperature in two different ways, with faster reduction at a high temperature greatly increasing the concentration of Pd atoms and hence the number of seeds formed in the nucleation step. At the same concentration of Pd precursor, an increase in the number of seeds resulted in the formation of smaller Pd nanoparticles. On the other hand, the dependence of reduction rate on temperature may also influence the reduction kinetics and hence the formation of nanoplates. As the temperature was increased, the shape of Pd nanostructures evolved from hexagon to triangle. For example, when the reaction was carried out under the same conditions as in the synthesis of hexagonal nanoplates except that the temperature was raised from 80 to 95 °C, the product was a mixture of hexagonal and triangular nanoplates of smaller sizes (Figure 6B).

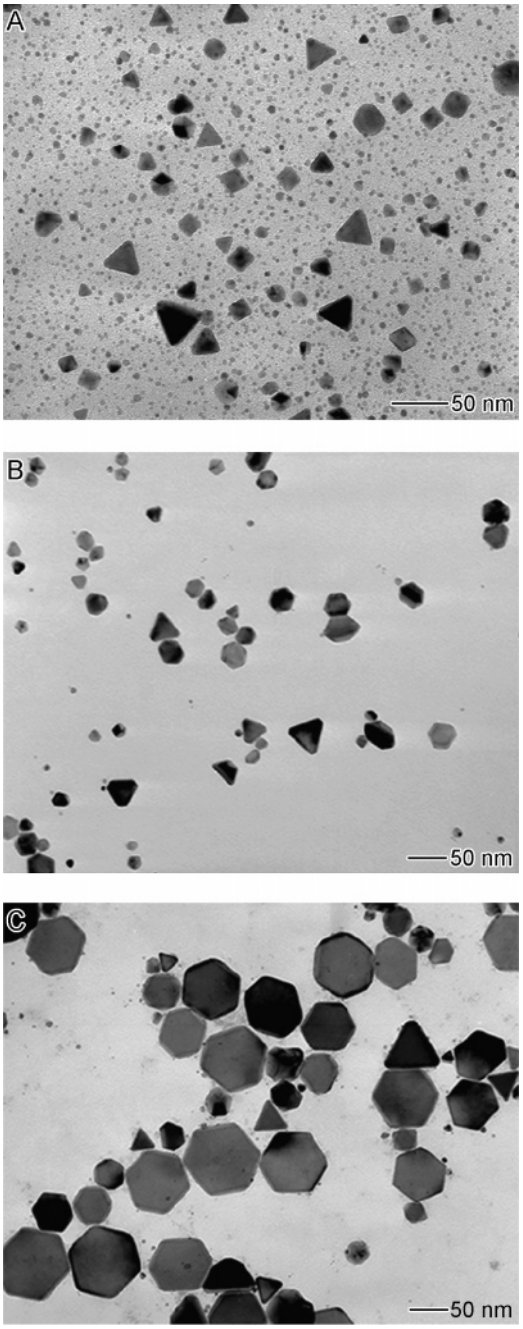

Figure 6. TEM images of Pd nanoparticles prepared under the same condition as in Figure 2A, except that (A) PVA (MW = 88 000) rather than PVP was added; (B) the reaction temperature was increased to 95 °C; and (C) the room light was completely blocked from the reaction system.

(24) (a) Watzky, M. A.; Finke, R. G. *J. Am. Chem. Soc.* **1997**, *119*, 10382. (b) Mallick, K.; Wang, Z. L.; Pal, T. *J. Photochem. Photobiol. A* **2001**, *140*, 75. (c) Ciacchi, L. C.; Mertig, M.; Pompe, W.; Meriani, S.; De Vita, A. *Platinum Metals Rev.* **2003**, *47*, 98. (d) Besson, C.; Finney, E. E.; Finke, R. G. *J. Am. Chem. Soc.* **2005**, *127*, 8179.

(25) Cotton, F. A.; Wilkinson, G. *Advanced Inorganic Chemistry*; Wiley: New York, 1999.

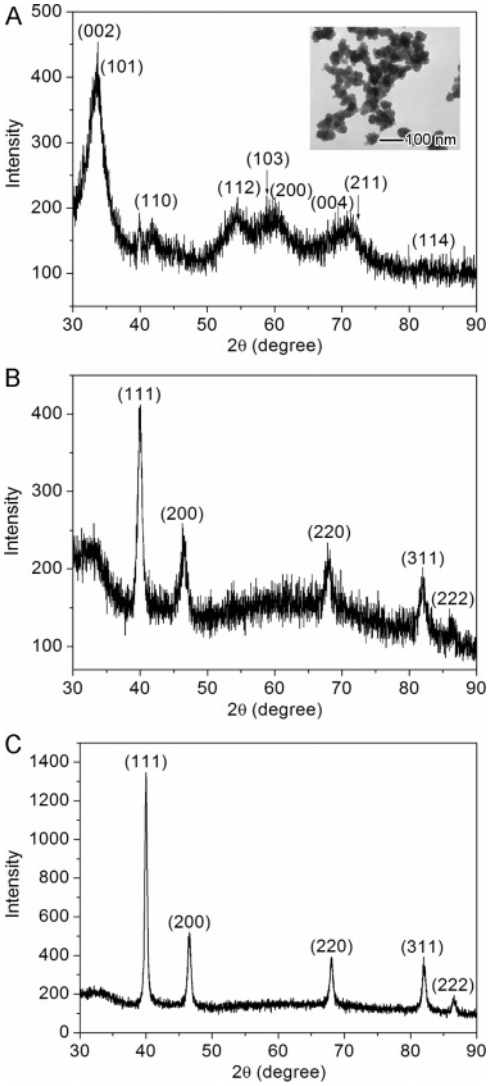

Figure 7. (A) XRD pattern of the product obtained in the absence of PVP. (Inset) TEM image of the corresponding sample. (B) XRD pattern of the product prepared with the molar ratio of PVP (MW = 55 000) to Na_2PdCl_4 being reduced to 1.5. (C) XRD pattern of the hexagonal nanoplates prepared with the molar ratio of PVP (MW = 55 000) to Na_2PdCl_4 being increased to 5.

In the previously reported synthesis of Ag nanoplates, light of appropriate wavelengths was found to be indispensable for the formation of plate morphology.[12] To examine this effect, we also performed a reaction by completely blocking light from the reaction system. As shown in ref 18, light was not critical to the formation of Ag nanoplates. Figure 6C shows a typical TEM image of a Pd sample prepared in the absence of light, for which we could not find significant difference in morphology as compared with the normal synthesis (Figure 2A). These results suggest that light is not required for the formation of either Ag or Pd nanoplates.

Formation of Gold Microplates. We have also prepared Au microplates using the same reduction chemistry. Figure 8A shows the SEM image of a sample synthesized with the molar ratio of PVP (MW = 29 000) to $HAuCl_4$ being kept at 15. This particular sample contained both triangular and hexagonal plates with edge lengths ranging from 600 nm to over 1 μm. Figure 8 panels B and C show TEM images and ED patterns taken from hexagonal and triangular plates, respectively. Both diffraction patterns are composed of three sets of diffraction spots with 6-fold rotational symmetry, which can be indexed to be the {422}, {220}, and

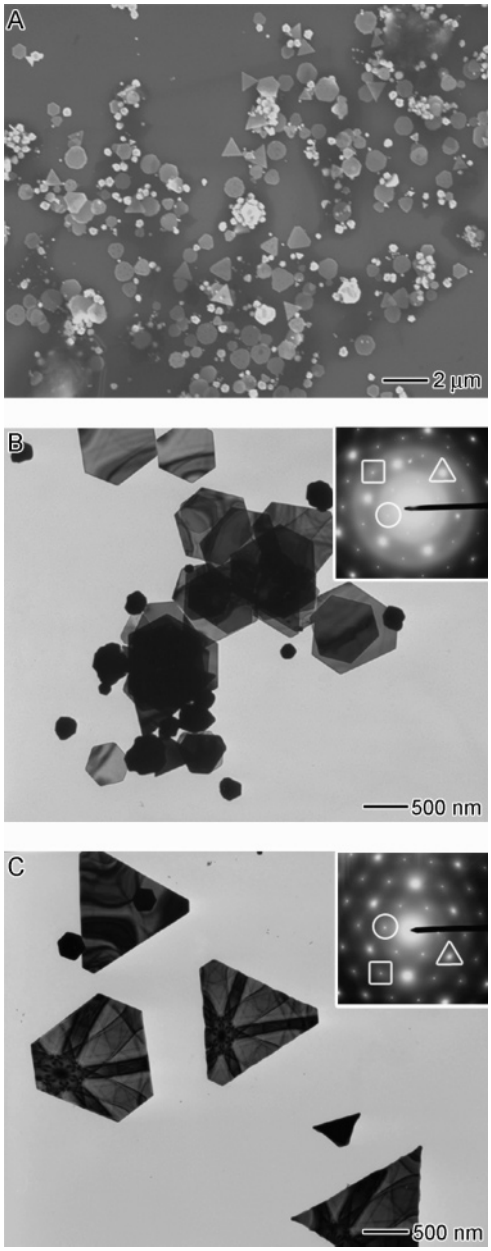

Figure 8. (A) SEM and (B) TEM images of Au microplates synthesized at 65 °C by reducing $HAuCl_4$ with the hydroxyl end groups of PVP. The PVP had an average molecular weight of 29 000, and its molar ratio (in terms of repeating unit) to $HAuCl_4$ was 15. (Inset) ED pattern taken by directing the electron beam perpendicular to the flat faces of a single hexagonal plate. (C) TEM image of the triangular plates mixed in the same batch of sample. (Inset) ED pattern taken by directing the electron beam perpendicular to the flat faces of a single triangular plate. The spots squared, triangled, and circled could be indexed to the {220}, {422}, and forbidden 1/3{422} reflections, respectively.

forbidden 1/3{422} reflections, respectively. These patterns indicate that the flat top and bottom faces of both Au hexagonal and triangular plates are also bound by the {111} planes.

It is worth noting that the molar ratio of PVP to $HAuCl_4$ and the molecular weight of PVPs also played a crucial role in the formation of Au microplates: when the molar ratio was higher than 15, the main products were aggregates of irregular nanoparticles instead of plates because of faster reduction. As the ratio dropped below 15, it was impossible to collect any precipitate.

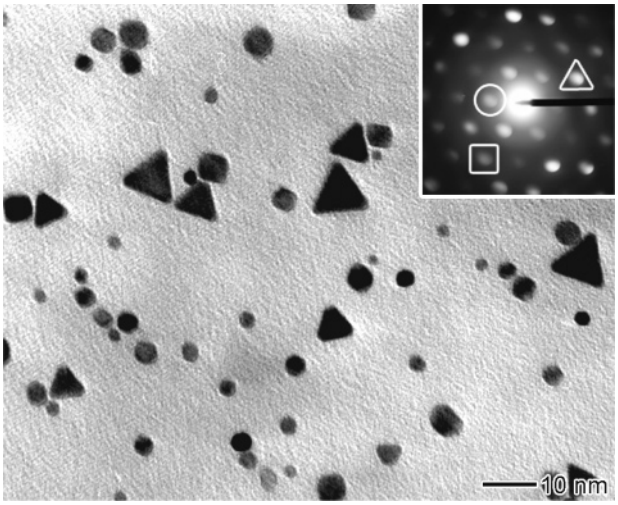

Figure 9. TEM image of Pt nanoparticles synthesized at 80 °C by reducing Na_2PtCl_4 with the hydroxyl end groups of PVP. The PVP had an average molecular weight of 55 000, and its molar ratio (in terms of repeating unit) to Na_2PtCl_4 was 5. (Inset) ED pattern taken by directing the electron beam perpendicular to the flat faces of a single nanoplate. The spots squared, triangled, and circled could be indexed to the {220}, {422}, and forbidden 1/3{422} reflections, respectively.

Other Metals. Reduction by the hydroxyl end groups of PVP can also be applied to other noble metals, albeit the major products were small nanoparticles rather than thin plates. For example, we used a similar process to generate Pt nanoparticles. The product consists of 15% triangular nanoplates and 85% small nanoparticles (see Figure 9). The ED pattern from a single nanoplate (inset, Figure 9) suggests that there also exist stacking faults in the Pt nanoplates. The low yield of nanoplates can be attributed to the difficulty in forming stacking faults inside a Pt nanocrystal. As described above, the formation of stacking faults is critical to the growth of thin nanoplates. For Pt nanocrystals, however, it is not favorable to incorporate twinned structures or stacking faults.[11b,26] As a result, the reduction of Pt salts by the hydroxyl end groups of PVP led to the formation of other shapes with high yields. For more active metals such as Fe, Co, Ni, and Cu, the reducing power of the hydroxyl end group is too weak to be used for their synthesis.

4. Conclusion

The hydroxyl end groups of PVP have been demonstrated as a mild reductant for synthesizing nanoplates made of noble metals such as Ag, Au, Pd, and Pt. Although the repeating unit of PVP has been extensively investigated for its ability to form coordination binding with a variety of metal surfaces, the end groups remain largely unexplored in terms of functionality and reactivity. The present work clearly demonstrates that the hydroxyl end groups of PVP (and possibly other kinds of polymers too) could reduce metal salts at a sufficiently slow rate so that the growth became kinetically controlled, leading to the formation of thin plates.

By varying the reaction time, the kinetically controlled synthesis has allowed us to produce metal plates with different (e.g., circular, hexagonal, and triangular) cross-sections, as well as tunable lateral dimensions from 50 to 500 nm. The SPR peaks of these metal plates could be tuned from the UV to the visible region. Thanks to their sharp corners and edges, the triangular nanoplates made of Ag are potentially useful as active substrates for SERS and related applications. It is also worth mentioning that the exceptional chemical sensitivity of Pd toward hydrogen should make its nanoplates especially useful for hydrogen storage and SPR-based sensing of hydrogen gas.[27] In addition, the small plates of noble metals might find use as catalysts, photothermal heating elements, absorption contrast agents, and chemically specific optical sensors.

This work suggests that one should never overlook the role and capability of a component commonly used in a conventional synthesis of colloidal nanocrystals. In comparison with other methods of kinetically controlled synthesis (e.g., photoinduced or thermally induced transformation and coupling with oxidative etching), the synthetic approach described in this article is much simpler and more versatile. Although the current work was focused on Ag, Au, Pd, Pt, and PVP, we believe that this new strategy is also applicable to other noble metals and organic polymers. It is expected that reduction of metal salts by the end groups of a polymer may eventually provide an environmentally benign and scalable route to shape-controlled synthesis of metal nanocrystals.

Acknowledgment. This work was supported in part by a grant from the NSF (DMR-0451788), a subcontract from the NSF-funded MERSEC program at the University of Washington, and a fellowship from the David and Lucile Packard Foundation. Y.X. is a Camille Dreyfus Teacher Scholar (2002−2007). I.W. was a visiting student from the Tokyo Institute of Technology and was partially supported by a research fellowship from the Japan Society for the Promotion of Science (JSPS) for Young Scientists. L.Z.-Y. was supported by the National Natural Science Foundation of China (10525419). This work used the Nanotech User Facility (NTUF), a member of the National Nanotechnology Infrastructure Network (NNIN) funded by the NSF.

LA061323X

(26) (a) Ahmadi, T. S.; Wang, Z. L.; Green, T. C.; Henglein, A.; El-Sayed, M. A. *Science* **1996**, *272*, 1924. (b) Ahmadi, T. S.; Wang, Z. L.; Henglein, A.; El-Sayed, M. A. *Chem. Mater.* **1996**, *8*, 1161. (c) Petroski, J. M.; Wang, Z. L.; Green, T. C.; El-Sayed, M. A. *J. Phys. Chem. B* **1998**, *102*, 3316. (d) Chen, J.; Herricks, T.; Geissler, M.; Xia, Y. *J. Am. Chem. Soc.* **2004**, *126*, 10854. (e) Herricks, T.; Chen, J.; Xia, Y. *Nano Lett.* **2004**, *4*, 2367.

(27) (a) Tobiška, P.; Hugon, O.; Trouillet, A.; Gagnaire, H. *Sens. Actuators* **2001**, *74*, 168. (b) Sun, Y.; Tao, Z.; Chen, J.; Herricks, T.; Xia, Y. *J. Am. Chem. Soc.* **2004**, *126*, 5940.